AFRL-RX-WP-JA-2014-0192

MODELING OF CROSS-PLANE INTERFACE THERMAL CONDUCTANCE BETWEEN GRAPHENE NANO-RIBBONS (POSTPRINT)

Ajit K. Roy
AFRL/RXAN

SEPTEMBER 2014
Interim Report

Distribution A. Approved for public release; distribution unlimited.

See additional restrictions described on inside pages

STINFO COPY

© 2014 IOP Publishing Ltd

AIR FORCE RESEARCH LABORATORY
MATERIALS AND MANUFACTURING DIRECTORATE
WRIGHT-PATTERSON AIR FORCE BASE, OH 45433-7750
AIR FORCE MATERIEL COMMAND
UNITED STATES AIR FORCE

NOTICE AND SIGNATURE PAGE

Using Government drawings, specifications, or other data included in this document for any purpose other than Government procurement does not in any way obligate the U.S. Government. The fact that the Government formulated or supplied the drawings, specifications, or other data does not license the holder or any other person or corporation; or convey any rights or permission to manufacture, use, or sell any patented invention that may relate to them.

This report was cleared for public release by the USAF 88th Air Base Wing (88 ABW) Public Affairs Office (PAO) and is available to the general public, including foreign nationals.

Copies may be obtained from the Defense Technical Information Center (DTIC) (http://www.dtic.mil).

AFRL-RX-WP-JA-2014-0192 HAS BEEN REVIEWED AND IS APPROVED FOR PUBLICATION IN ACCORDANCE WITH ASSIGNED DISTRIBUTION STATEMENT.

//Signature//

AJIT K. ROY
Nanoelectronic Materials Branch
Functional Materials Division

//Signature//

DIANA M. CARLIN, Chief
Nanoelectronic Materials Branch
Functional Materials Division

//Signature//

TIMOTHY J. BUNNING, Chief
Functional Materials Division
Materials and Manufacturing Directorate

This report is published in the interest of scientific and technical information exchange, and its publication does not constitute the Government's approval or disapproval of its ideas or findings.

REPORT DOCUMENTATION PAGE

Form Approved
OMB No. 074-0188

Public reporting burden for this collection of information is estimated to average 1 hour per response, including the time for reviewing instructions, searching existing data sources, gathering and maintaining the data needed, and completing and reviewing this collection of information. Send comments regarding this burden estimate or any other aspect of this collection of information, including suggestions for reducing this burden to Defense, Washington Headquarters Services, Directorate for Information Operations and Reports, 1215 Jefferson Davis Highway, Suite 1204, Arlington, VA 22202-4302. Respondents should be aware that notwithstanding any other provision of law, no person shall be subject to any penalty for failing to comply with a collection of information if it dows not display a currently valid OMB control number. PLEASE DO NOT RETURN YOUR FORM TO THE ABOVE ADDRESS.

1. REPORT DATE (DD-MM-YYYY)	2. REPORT TYPE	3. DATES COVERED *(From – To)*
September 2014	Interim	08 June 2011 – 07 August 2014

4. TITLE AND SUBTITLE
MODELING OF CROSS-PLANE INTERFACE THERMAL CONDUCTANCE BETWEEN GRAPHENE NANO-RIBBONS (POSTPRINT)

5a. CONTRACT NUMBER
In-House

5b. GRANT NUMBER

5c. PROGRAM ELEMENT NUMBER
61102F

6. AUTHOR(S)
(see back)

5d. PROJECT NUMBER
2305

5e. TASK NUMBER

5f. WORK UNIT NUMBER
X091

7. PERFORMING ORGANIZATION NAME(S) AND ADDRESS(ES)
(see back)

8. PERFORMING ORGANIZATION REPORT NUMBER

9. SPONSORING / MONITORING AGENCY NAME(S) AND ADDRESS(ES)
Air Force Research Laboratory
Materials and Manufacturing Directorate
Wright Patterson Air Force Base, OH 45433-7750
Air Force Materiel Command
United States Air Force

10. SPONSOR/MONITOR'S ACRONYM(S)
AFRL/RXAN

11. SPONSOR/MONITOR'S REPORT NUMBER(S)
AFRL-RX-WP-JA-2014-0192

12. DISTRIBUTION / AVAILABILITY STATEMENT
Distribution A. Approved for public release; distribution unlimited. This report contains color.

13. SUPPLEMENTARY NOTES
PA Case Number: 88ABW-2014-1702; Clearance Date: 14 April 2014. Journal article published in 2D Materials 1 (2014) 025005 053-1583/14/025005+16. © 2014 IOP Publishing Ltd. The U.S. Government is joint author of the work and has the right to use, modify, reproduce, release, perform, display or disclose the work. The final publication is available at http://dx.doi.org/10.1088/2053-1583/1/2/025005.

14. ABSTRACT
Using non-equilibrium molecular dynamics for thermal energy transfer, we investigate the interfacial thermal conductance between non-covalently interacting graphene nano-ribbons (GNRs) of varying lengths and widths in a cross-contact (x-shaped) geometry. Our results show that the out-of-plane conductance between GNRs can vary significantly (up to a factor of 4) depending upon their geometric parameters. We observe that when plotted against aspect ratio, the predicted interface thermal conductance values fit excellently on a single masterplot with a logarithmic scaling, suggesting the importance of GNR aspect ratio towards thermal conductance. We propose a model based on incorporating different thermal conductance characteristics of edge and inner interacting regions which predicts the observed logarithmic dependence on aspect ratio. We also study the effect of graphene edge roughness, temperature, and strain on out-of-plane thermal conductance and discuss the observed results based on local vibrational characteristics of atoms within interacting region, number of interacting phonons, and the degree to which they interact across the interaction zone.

15. SUBJECT TERMS
molecular dynamics, graphene nano-ribbons, interface thermal conductance, edge roughness, tensile strain, temperature dependence

16. SECURITY CLASSIFICATION OF:			17. LIMITATION OF ABSTRACT	18. NUMBER OF PAGES	19a. NAME OF RESPONSIBLE PERSON *(Monitor)*
					Ajit K. Roy
a. REPORT	b. ABSTRACT	c. THIS PAGE			19b. TELEPHONE NUBER *(include area code)*
Unclassified	Unclassified	Unclassified	SAR	20	(937) 255-9034

Standard Form 298 (Rev. 2-89)
Prescribed by ANSI Std. Z39-18

REPORT DOCUMENTATION PAGE Cont'd

6. AUTHOR(S)

Ajit K. Roy, Barry L. Farmer, Andrea A. Voevodin - Materials and Manufacturing Directorate, Air Force Research Laboratory, Functional Materials Division

Vikas Varshney, Jonghoon Lee - Universal Technology Corporation

7. PERFORMING ORGANIZATION NAME(S) AND ADDRESS(ES)

AFRL/RXAN
Air Force Research Laboratory
Materials and Manufacturing Directorate
Wright-Patterson Air Force Base, OH 45433-7750

Universal Technology Corporation
1270 N. Fairfield Rd.
Dayton, OH 45432-2600

2D Materials

Modeling of cross-plane interface thermal conductance between graphene nano-ribbons

Vikas Varshney[1,2], Jonghoon Lee[1,2], Barry L Farmer[1], Andrey A Voevodin[1] and Ajit K Roy[1]

[1] Materials and Manufacturing Directorate, Air Force Research Laboratory, Wright-Patterson AFB, Dayton, OH 45433-7500, USA
[2] Universal Technology Corporation, 1270 N. Fairfield Rd., Dayton, OH 45432-2600, USA
E-mail: vikas.varshney@wpafb.af.mil and ajit.roy@us.af.mil

Received 7 March 2014, revised 2 July 2014
Accepted for publication 7 August 2014
Published 19 September 2014

2D Materials **1** (2014) 025005

doi:10.1088/2053-1583/1/2/025005

Abstract

Using non-equilibrium molecular dynamics for thermal energy transfer, we investigate the interfacial thermal conductance between non-covalently interacting graphene nano-ribbons (GNRs) of varying lengths and widths in a cross-contact (x-shaped) geometry. Our results show that the out-of-plane conductance between GNRs can vary significantly (up to a factor of 4) depending upon their geometric parameters. We observe that when plotted against aspect ratio, the predicted interface thermal conductance values fit excellently on a single master-plot with a logarithmic scaling, suggesting the importance of GNR aspect ratio towards thermal conductance. We propose a model based on incorporating different thermal conductance characteristics of edge and inner interacting regions which predicts the observed logarithmic dependence on aspect ratio. We also study the effect of graphene edge roughness, temperature, and strain on out-of-plane thermal conductance and discuss the observed results based on local vibrational characteristics of atoms within interacting region, number of interacting phonons, and the degree to which they interact across the interaction zone.

S Online supplementary data available from stacks.iop.org/TDM/1/025005/mmedia

Keywords: molecular dynamics, graphene nano-ribbons, interface thermal conductance, edge roughness, tensile strain, temperature dependence

© 2014 IOP Publishing Ltd

Distribution A. Approved for public release; distribution unlimited.

Introduction

Technological advancements in fabrication at 'nano' length scales over the past decade have opened up a gamut of opportunities for development of next generation nanoelectronics, such as nano-electromechanical systems [1, 2], nano integrated circuits [3], thermoelectric devices [4, 5], thermal rectifiers [6], and others. As this exciting field continues to evolve towards fabrication of next generation microscale and nanoscale devices, anticipated and un-anticipated challenges are evolving as well. Due to the much larger surface area to volume ratio in such small devices, power dissipation at interconnects emerges as one of the most crucial concern towards determining device efficiency, performance predictability, and reliability. The energy transfer through these contacts occurs via conduction electrons and thermal vibrations, as well as their mutual interaction. This transfer is often characterized as electrical contact resistance (for electrons), interface thermal resistance (for heat) and electron-phonon coupling, respectively. In an operating device, these resistances collectively govern the current flow, control temperature distribution within the device, influence detrimental hot spots, and thus dictate its performance.

Owing to excellent thermal and electrical properties, carbon nanostructures offer a novel and cost effective route towards designing next generation nano-electronic devices. Moreover, it is often reported that these properties can be tuned through different chemical and structural modifications (such as functionalization, dopants, defects, etc) [7–10]. Of particular interest to this study is the issue of interface thermal conductance (ITC) across carbon based nanostructures, which is associated with the vibrational energy transfer at the interface (its inverse is termed as interface thermal resistance). In carbon based electronics, such interfaces either involve dissimilar material contacts, such as carbon nanotube or graphene interacting with other metals or semi-conductors (also known as hetero-contact) [11, 12], or involve similar material contact, such as CNT-CNT cross contact within CNT-mesh in a CNT based nanoelectronics [13–15].

Within the framework of similar material contacts comprised of carbon nanostructures, several groups, both experimentally [16–21] and through simulations [22–33], have investigated thermal interface conductance (or resistance) at CNT-CNT and graphene-graphene interfaces over the past decade. The studies offer insights into thermal transport across such interfaces, and how it can be tuned by modifying the interface properties through alignment [23], surrounding environment [26–28], possible metallization [34], functionalization [32, 35], etc. Nevertheless, very few studies have explored out-of-plane thermal conductance between graphene layers, which are interacting through van der Waals forces [20, 28–31]. Most of the graphene thermal conductance research has been focused either on in-plane transport of graphene (such as effect of grain boundaries or defects on in-plane thermal conductance at the defected interface) [36] or on graphene thermal conductance at hetero-contacts (such as a graphene monolayer supported on different metallic/semiconducting substrates) [37–39]. Furthermore, to the best of our knowledge, no study has focused on exploring interfacial thermal conductance across single-layer graphene nano-ribbons (GNRs).

The current study uses non-equilibrium molecular dynamics (NEMD) simulations to investigate whether intrinsic GNR characteristics (length, width, edge features) and external stimuli (tensile strain, temperature) can affect the thermal energy transport across the GNR contacts, and if so, to what degree. The understanding of these out-of-plane thermal properties and contact energy transport shall provide a guiding role towards determining graphene based

Distribution A. Approved for public release; distribution unlimited.

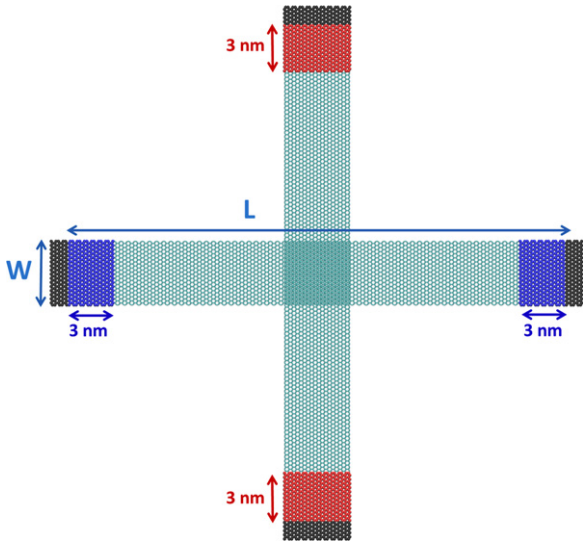

Figure 1. Schematic of a representative x-shaped GNR pair as considered in this study. *L* and *W* represent the length and width of the nano-ribbon, respectively. Color scheme: fixed carbon atoms (black); hot thermostated carbon atoms (red); cold thermostated carbon atoms (blue); unthermostated carbon atoms (cyan).

device inter-connect specifications and GNR junctions to optimize device performance, achieve predictable operation, and reliability in the use.

Simulation methodology

Simulation setup

Figure 1 shows a representative system of X-shaped geometry made from two perpendicular GNRs. First, a bi-layer graphene system was generated using Materials Studio with planar dimensions of 120×120 nm and an inter-layer spacing of 3.4 Å. Next, two perpendicular ribbons were carved out using an in-house script with the desired length (L) and width (W) as shown in figure 1. For the investigation of length/width dependence on thermal conductance, several systems were generated where L was varied from 10 to 100 nm and W was varied from 2 to 20 nm. All simulations were performed using LAMMPS molecular dynamics software [40] using the PCFF force field [41]. This force field has been successfully employed for the investigation of thermal conductance/conductivity in several elemental carbon related studies [42–48]. After an initial minimization, all systems were subjected to NVT (canonical ensemble) simulations for equilibration for 200–500 ps (depending upon the system size) where both edges (1 nm) at ends of both GNRs (shown as black in figure 1) were fixed. During the equilibration stage, a timestep of 1 fs was used for the simulations. As the length of the GNR was fixed, the initial C-C bond lengths were adjusted to make sure that there was no residual tensile/compressive stress/strain within the GNR during equilibration by monitoring different pressure

Distribution A. Approved for public release; distribution unlimited.

components[3]. We also studied the effect of temperature as well as tensile and compressive strain on interfacial thermal conductance for a representative bi-layer GNR system. Later in the text, it is shown that such modulation of external stimuli can lead to significant modification of interfacial heat flow.

Thermal transport simulations

After equilibration, NEMD simulations were used to calculate thermal conductance across GNR cross-plane interfaces. For these simulations, the edges (~1 nm) on both ends of the two perpendicular GNRs were kept fixed. To introduce a temperature drop (or discontinuity) at the interface interacting through van der Waals interactions, 3 nm sections near both ends were thermostated at either 350 K (hot GNR) or 250 K (cold GNR) for all studied cases as shown in figure 1. All simulations were performed with a timestep of 0.5 fs under the NVE (microcanonical) ensemble. To investigate possible artifacts caused by the choice of thermostat, several thermostat schemes were tested with heating/cooling either at the boundaries or throughout the whole GNR as well as using several thermostating schemes (Nose–Hoover or temperature rescaling) with different adjustable parameters associated with each scheme. However, only a slight difference in estimated thermal conductance was observed with no statistically significant scattering or trends, as also reported previously [49]. For all the results presented, we used the temperature rescaling approach in the thermostated regions with the rescaling frequency of 100 timesteps. Once steady state was reached (~500 ps), two different forms of interface thermal conductance calculated using the following set of equations

$$\Lambda_1 = \frac{Q}{\Delta T};\ \Lambda_2 = \frac{Q}{A_{\mathrm{GNR}}\,\Delta T}\ , \tag{1}$$

where Λ_1 (pW/K) and Λ_2 (MW/m^2-K) are total and area-normalized ITC, respectively, Q is the heat flow rate, ΔT is the temperature difference between the two GNRs at the interface contact (overlapped region), and A_{GNR} is the overlapping area of interaction at the GNR contact. For detailed discussion of the estimation of this area, please refer to supporting information S1. The heat flow rate Q was calculated as follows

$$\frac{Q}{A\Delta t} = \frac{1}{A\Delta t}\left\langle \frac{1}{2}\sum_{k=1}^{N_B} m_k\left(v_k^2 - vp_k^2\right)\right\rangle\ , \tag{2}$$

where vp_k and v_k are the velocities of the thermostated (either hot or cold) atoms before and after the rescaling to desired temperature, respectively and N_B is the number of atoms in the thermostated region.

[3] In order to achieve zero planar residual strain for our systems of interest, a test case of nano-ribbon was run with different initial C-C bond lengths (between 1.41 and 1.43) at 300K and planar pressure was monitored. Based on these simulations, the case with ~zero planar pressure was used as standard C-C length for all studied simulations presented.

Distribution A. Approved for public release; distribution unlimited.

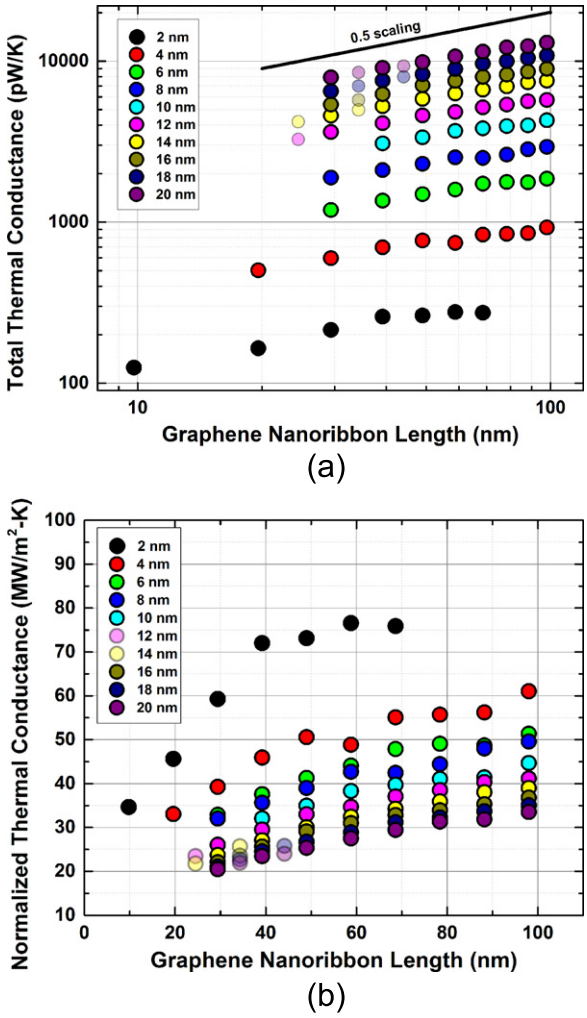

Figure 2. (a) Total thermal conductance (pW/K) and (b) area-normalized thermal conductance (MW/m^2-K) across different studied GNRs, plotted as a function of GNR length for different widths. A power law scaling of ½ is shown in (a) as a guide to the eye. Semi-transparent data represent additional simulations (not discussed in text) to further confirmation of the observed trends.

Results and discussion

Effect of GNR length & width

Figure 2(a) plots the total thermal conductance (Λ_1) as a function of GNR length for different studied widths. A few additional GNR systems were modeled (in addition to what is described in the simulation methodology) for a better estimate of thermal conductivity trends, and are shown in light shaded colors[4]. A power-law scaling of ½ is also plotted as a guide for the eye. As expected, the figure clearly shows that for constant GNR length, the total thermal

[4] Additional simulations were performed to validate the aspect ratio trend, especially at the lower aspect ratio, as shown in figure 2. For wider GNRs, 10 nm and 20 nm simulation data points are missing due to system constraints, e.g. it is impossible to model 20 nm wide GNR with only 10 nm length.

Distribution A. Approved for public release; distribution unlimited.

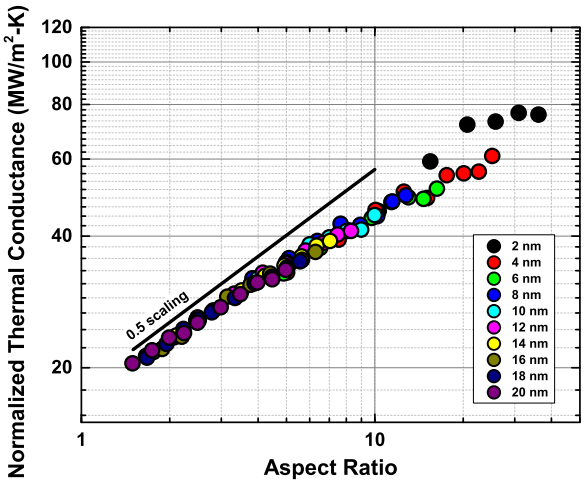

Figure 3. Plot of the area-normalized thermal conductance as a function of aspect ratio (η) for different studied GNRs on a log-log scale. A power law scaling of ½ is shown as a guide to the eye.

conductance increases monotonically with increase in GNR width. This increase can be attributed to the larger area of overlap between the crossed-over GNRs. More importantly, the figure also shows that for all cases, the total thermal energy exchange (and thus Λ_1) increases as well with GNR length for a constant GNR width. As discussed later, this increase is attributed to an increased role of GNR edges towards inter-graphene coupling with the increase in length. It is also evident from this figure that Λ_1 has a sub-½ power law *like* scaling with respect to the GNR length.

Figure 2(b) plots the discussed data from the perspective of an area-normalized thermal conductance (Λ_2). Interestingly, this figure details several interesting and key observations. For physically interacting GNRs as investigated in this study, one would expect the normalized conductance to be somewhat independent of the overlapping area and nano-ribbons parameters. However, the figure clearly shows that a single value of normalized thermal conductance is not valid but ranges between ~20–70 MW/m^2 K for the studied cases. Moreover, the figure shows that the Λ_2 increases with GNR length (for a constant width) and decreases with GNR width (for a constant length). The decrease in Λ_2 for a constant GNR length suggests that if one increases the overlap area by a constant factor (by increasing GNR width), the increase in thermal energy exchange is less than proportional to the contact area increase (Please see below for further discussion). Overall, it is quite clear from figure 2 that cross-plane thermal conductance values (both Λ_1 and Λ_2) between GNRs are strongly dependent on their dimensions.

Thermal conductance versus aspect ratio

From the observed Λ_1 and Λ_2 dependences on L and W of the GNRs in contact, it is reasonable to propose that the aspect ratio (η) should be an important parameter associated with thermal transport at the contact interface. In this context, thermal conductance data in figure 2 was re-analyzed as a function of aspect ratio and is shown in figure 3 for area-normalized thermal conductance. A similar plot for total thermal conductance versus η did not add any additional insights and is provided in the supporting information S2 for reader's interest. The aspect ratio for the studied cases was calculated using the following equation

Distribution A. Approved for public release; distribution unlimited.

$$\eta = \frac{L'}{\sqrt{A_{\mathrm{GNR}}}}\ , \tag{3}$$

where L' is the length (in nm) of the GNR excluding fixed ends and A_{GNR} is the effective area (in nm^2) of contact between GNRs (Please see supporting information S1 for calculation of A_{GNR}).

It is fascinating to observe that when Λ_2 is plotted with respect to aspect ratio (unlike length or width), all the data points fall on a single master plot up to the aspect ratio of ~20. The figure clearly shows that the aspect ratio of the GNR is, in fact, the governing parameter which determines the extent of thermal energy exchange between GNRs. For example, in accordance with the trend in figure 3, for two different size GNRs with same aspect ratio (e.g. with dimensions $W \times L = 4 \times 40$ nm and $W \times L = 8 \times 80$ nm), we found Λ_2 to be 45.5 and 44.5 MW/m^2 K respectively. In addition, the associated per unit area thermal energy exchange was observed to be 0.50 and 0.53 MW/m^2 respectively.

Figure 3 also shows a power law scaling *guideline* of ½. While at low aspect ratios, the scaling of ½ seems fitting, it shows a considerable deviation at higher aspect ratios. In order to get a better understanding of normalized conductance with respect to aspect ratio, we tested the fit of the data with several functional forms. The two most appropriate fits among those are shown in figures 4(a) and 4(b), namely, the power fitting and a three-parameter logarithmic fitting, respectively. The corresponding equations and fitting exponents are also shown in the respective figures. For power fitting (figure 4(a)), a much smaller exponent (0.38) than ½ is observed when fitted against all data points. Moreover, it is easy to observe clear deviations of the data points with respect to the power-law fitting line. Most of the middle data points reside above the fitting line, while the ones on the extremes are below the line. On the other hand, the logarithmic fitting (figure 4(b)) seems to provide a better overall fitting. The quality of the fit can also be gauged by comparing the fitting exponents for a full dataset fit with fittings done over a smaller window. Such fittings are reported in supporting information S3 for power and logarithmic fittings, respectively. It is seen that the logarithmic fitting on partial data fits results in the same coefficients when compared to a full fit while a clear distinction is observed for power law fitting (coefficient a monotonically increases from 16.13 to 21.89 while coefficient b decreases from 0.5 to 0.31), further validating the previous discussion. Moreover, based on functional form, it is easy to comprehend that a logarithmic fitting leads to a better asymptotic fit at larger aspect ratios (~20–100), where the thermal conductance is expected to saturate.

Proposed phenomenological model

We propose the following phenomenological model to qualitatively appreciate the dependence of ITC on aspect ratio as well as its logarithmic nature. In our model, the ITC (Λ_2) is *effectively* a weighted average of two limiting thermal conductance values, Λ_{i} and Λ_{o}. Here, sub-scripts i and o refer to the thermal conductance due to inner and outer interacting regions, respectively, and are also shown in figure 5. In our model, Λ_{i} refers to the intrinsic thermal conductance across bi-layer graphene in the limit of no edges, i.e. $\eta \sim 1$ or large bi-layer graphene flakes. On the other hand, Λ_{o} corresponds to thermal conductance, when a GNR 'edge' dominates the thermal interaction with the other GNR. Due to the greater flexibility, i.e. less constrained out-of-plane vibrations of edge atoms than atoms in the inner interaction region, we assume that edges can couple with other GNR to a stronger degree, resulting in a higher limiting value of Λ_{o} than Λ_{i}. The differences in vibrational properties of inner and edge atoms are also highlighted in

Distribution A. Approved for public release; distribution unlimited.

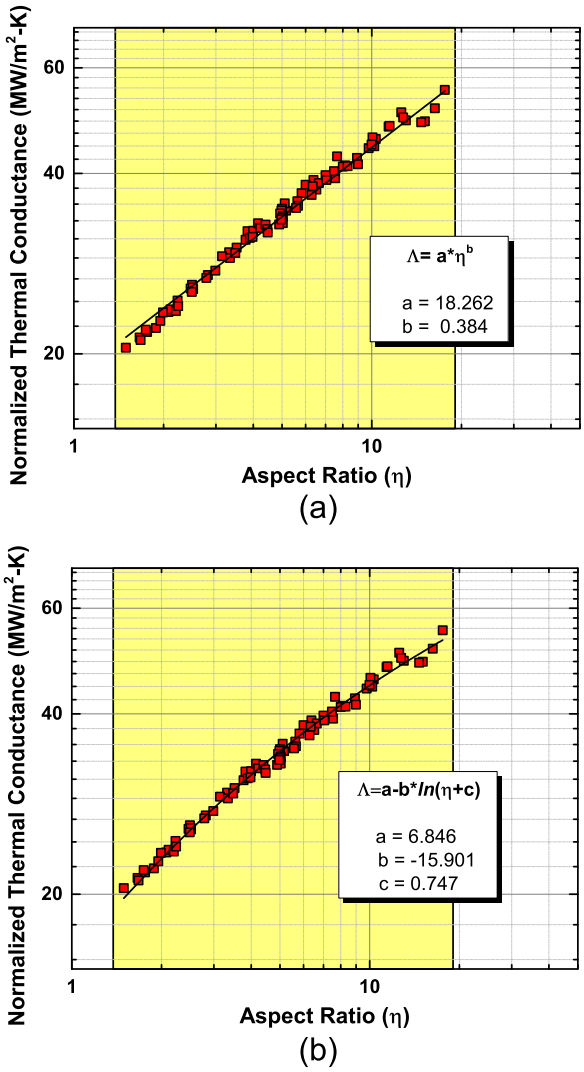

Figure 4. Graphs showing (a) power fitting and (b) logarithmic fitting of area-normalized thermal conductance (Λ_2) data sets with respect to aspect ratio (η). The equations along with derived parameters are also listed in the respective graphs. Please refer to figures S3a and S3b in the supporting information for comparing the derived parameters with partial fitting of the data set.

figure 6 as a power spectra for a representative system, calculated from the Fourier transform of the velocity auto-correlation function. The figure clearly shows the shift of vibrational spectrum to lower frequencies for edge atoms (especially ZO mode which occurs around ~20 THz and is responsible for out of plane vibrations), validating the greater degree of vibrational flexibility.

We also foresee a length l_d (shown in figure 5) from the GNR edge over which the thermal energy exchange is dominated through edges, i.e. Λ_o. We will refer to l_d as decay length as it indicates a length scale over which the effect of edge vibrational characteristics is noticeable. Within this framework, the *effective* ITC (Λ_2) can be calculated using the following equation of geometric averaging in terms of l_d, W, Λ_i and Λ_o.

Distribution A. Approved for public release; distribution unlimited.

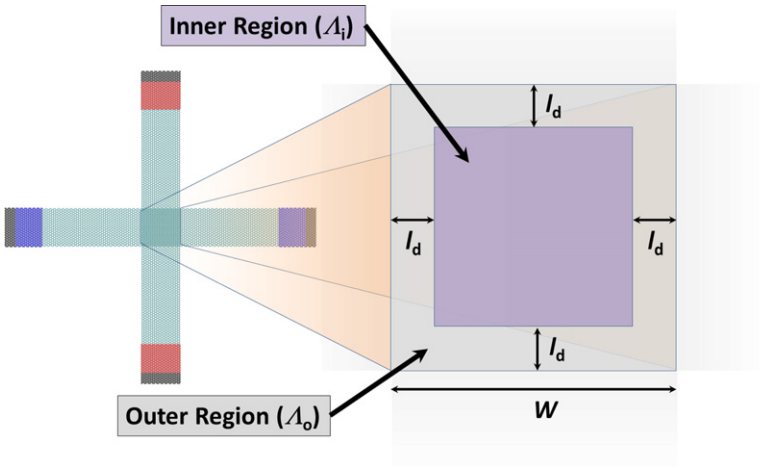

Figure 5. Schematic showing interaction (or overlap) region and identifying the inner and outer regions and their respective thermal conductance parameters (Λ_i and Λ_o). l_d is the decay length over which the effect of the edges become negligible.

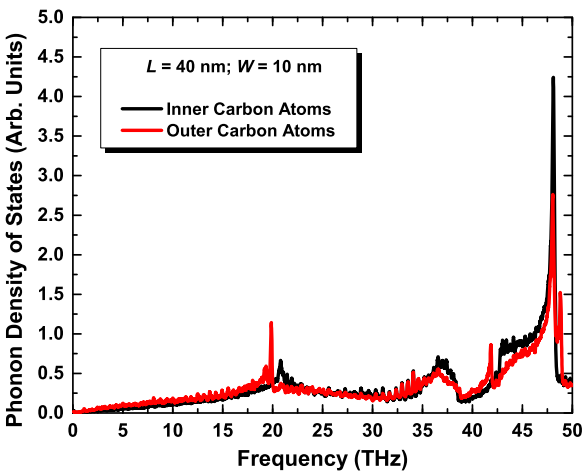

Figure 6. Plot of phonon density of states versus frequency for carbon atoms in inner (black) and outer (red) interaction regions for a representative system ($L = 40$ nm and $W = 10$ nm) with aspect ratio of 4.

$$\Lambda_2 = \frac{\Lambda_i \times \left(W - 2l_d\right)^2 + 2\Lambda_o\left(W \times l_d\right) + 2\Lambda_o\left(\left(W - 2l_d\right) \times l_d\right)}{W^2}. \tag{4}$$

In the limit, when l_d is significantly smaller than W, equation (4) can be simplified as

$$\Lambda_2 = \Lambda_i + \frac{2l_d}{W}\left(2\Lambda_o - \Lambda_i\right). \tag{5}$$

We assume that the decay length is not constant and is a function of both L and W. It is expected that for a constant W, $l_d \propto f(L)$ as the effect of edges towards thermal energy exchange is expected to penetrate deeper into the interacting region with increasing distance (L) between

Distribution A. Approved for public release; distribution unlimited.

the interaction region and the fixed (constrained) GNR ends, due to the greater degree of edges' out-of-plane flexibility. Moreover, when η becomes unity, l_d is expected to vanish since there would not be edges, and hence no decay length. One function which satisfies both conditions is a logarithmic function. Here, $l_d \propto \ln(L/W)$ or $l_d \propto \ln(\eta)$. This functional form suggests that for constant W, the decay length increases 'logarithmically' with distance between the fixed constraints.

From the ITC results, it is also observed that the relative contributions from Λ_i and Λ_o remains similar at certain constant η. In order to accommodate that, l_d should linearly increase with W when aspect ratio is constant. This linear proportionality of l_d with W is also in accordance with the need of additional length dimension in $l_d \propto \ln(\eta)$ with respect to dimensional equality of left- and right-hand side of the equations. Overall, we propose that $l_d \propto W\ln(\eta)$ or $l_d/W = \mu\ln(\eta)$ where μ is a dimensionless coefficient of proportionality. Putting this form in equation (5), we get

$$\Lambda_2 = \Lambda_i + 2\mu\left(2\Lambda_o - \Lambda_i\right)\ln(\eta). \tag{6}$$

As can be seen, equation (6) is very similar to fitted equation in figure 4(b) and showcases the observed logarithmic dependence when $l_d << W$ and secondary terms can be ignored, which in general holds true for small aspect ratio systems. When, l_d is comparable to W (higher aspect ratios), the secondary terms originating from 4 corners (see equation (4)) should not be ignored. In such cases, equation (6) can be derived to be

$$\Lambda_2 = \Lambda_i + 2\mu\left(2\Lambda_o - \Lambda_i\right)\ln(\eta) - 4\mu^2\left(\Lambda_o - \Lambda_i\right)(ln(\eta))^2 . \tag{7}$$

Although the functional form in equation (7) is not similar to the fitted form in figure 4(b), it does provide the saturation of Λ_2 at higher aspect ratios. With regards to prediction of Λ_i in limiting case of $\eta \sim 1$ (negligible contributions from the edges), the extrapolation of three-parameter logarithmic fitting lead to estimated value of 15.71 MW/m^2-K, which is also in good agreement with what is reported in the literature [28]. Furthermore, based on observed trends, we expect the intrinsic value of ITC Λ_o to be ~70 MW/m^2-K.

We should point out that the derivation of our proposed model is phenomenological in nature and is proposed for appreciating observed trends and provide a qualitative understanding of the features which are important across the interacting zone.

Effect of edge roughness

Previous discussion suggests that the vibrational freedom of GNR edges do play an important role in determining the decay length and eventually the total thermal energy exchange across the interacting bi-layer GNR interface. Hence, it is imperative to investigate the potential role of edge roughness towards out-of-plane thermal energy exchange. In this regard, we simulated ITC across a representative rough GNR for different lengths L between fixed constraints, but similar interacting area, as depicted in figure 7. As seen in the schematic, although the GNR is significantly *rough* with regards to transmitting in-plane phonons, the interacting zone was kept to be pristine and crossing at 90° in order to compare the results with rectangular (non-rough) GNR studies. Figure 7 also shows the calculated thermal conductance (Λ_2) values across rough GNRs as a function of aspect ratio and compare them with Λ_2 values corresponding to rectangular GNRs (shown as partially transparent data points). The figure shows that the rough GNR thermal conductance values match excellently with those with rectangular GNRs,

Distribution A. Approved for public release; distribution unlimited.

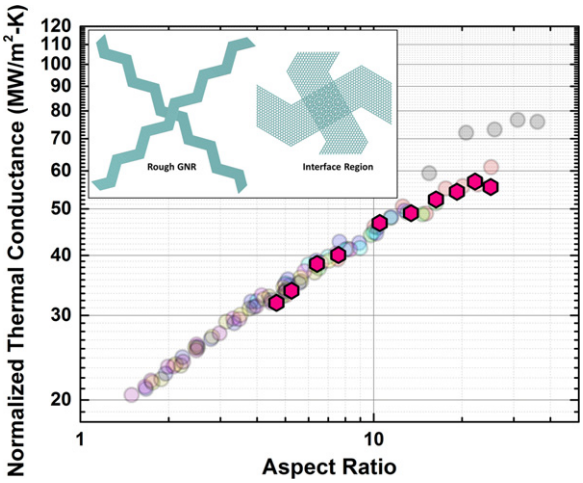

Figure 7. Plot of area-normalized interface thermal conductance as a function of aspect ratio (pink hexagons), showing the effect of overall graphene roughness on the thermal energy exchange across the interface. The top-inset shows both the overall structure of rough GNR as well as the structure interaction region. The partially transparent data points correspond to thermal conductance values of studied rectangular GNRs as discussed in figure 3.

suggesting that overall zigzag morphology of the GNR do not play a role towards out of plane thermal conductance across GNRs. In other words, a decrease in overall in-plane thermal conduction properties (for example, due to roughness) does not directly imply better out-of-plane conduction. Furthermore, it is observed that the interacting zone between GNRs is the same for both rough and rectangular GNRs and leads to similar values of Λ_2. Based on these observations, we argue that the out-of-plane thermal energy exchange depends predominantly on local vibrational characteristics of the interacting atoms, rather than overall roughness features of GNRs. Comparing rough and rectangular GNR cases, it can also be argued that the said local vibrational characteristics depends more significantly on the L (distance between the constraints) and W (GNR width), but not so much on overall roughness features of GNRs. However, we hypothesize that if the interaction region is modeled to be rough as well (which is not investigated here), a different scaling could emerge as it would modify the decay length characteristics, such as switching from a pristine one-dimensional character (perpendicular to the edge) to some different decay characteristics with higher degree of complexity (such as its dependence on degree of roughness).

Effect of temperature

To investigate the effect of temperature on thermal conductance across the GNR contact, we simulated a representative system with L and W correspond to 60 nm and 10 nm, respectively at different temperatures values for hot and cold thermostats, using the same NEMD methodology discussed in the text. In this context, figure 8 plots the calculated ITC (Λ_2) values for different equilibrated temperature. It is clear from the figure that the Λ_2 increases with temperature and could be explained using an argument based on the number of interacting phonons. While the aspect ratio was not altered for this study (effect of temperature), the number of phonons interacting across the interface increase (decrease) with increase (decrease) in temperature.

Distribution A. Approved for public release; distribution unlimited.

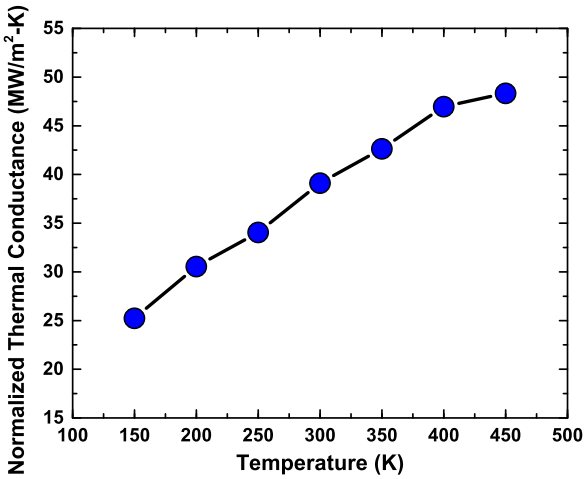

Figure 8. Plot of area-normalized interface thermal conductance versus temperature as studied for a representative cross shaped geometry of 60 nm long and 10 nm wide GNRs.

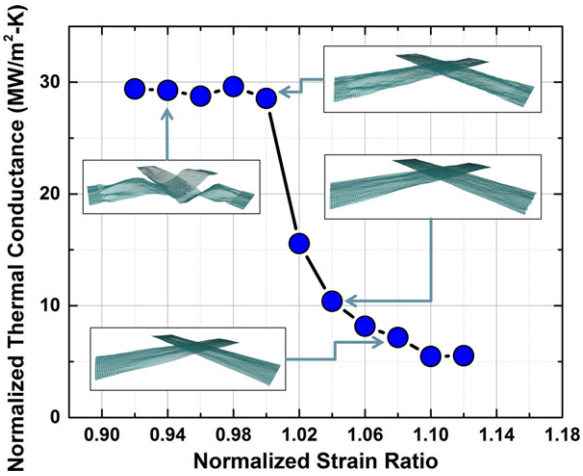

Figure 9. Plot of area-normalized thermal conductance across 40 nm long and 10 nm wide GNR as a function of compressive (<1.0) and tensile (>1.0) strain values.

Furthermore, the mean free path of the phonons becomes longer at a lower temperature due to lower number of phonons and a lesser number of in-plane anharmonic phonon-phonon scattering events. We foresee that such an increase in the mean free path would lower the phonon interaction time across the GNR contact and vice-versa. We believe that both discussed points contribute towards increasing (decreasing) the intrinsic values of both Λ_1 and Λ_0 with increase (decrease) in temperature, which in turn results in shown variation (figure 8) in effective ITC with temperature.

Effect of tensile & compressive strain

Figure 9 shows the predicted values of normalized thermal conductance (Λ_2) for different degrees of compressive and tensile strain with respect to unstrained GNR. Also shown in the

Distribution A. Approved for public release; distribution unlimited.

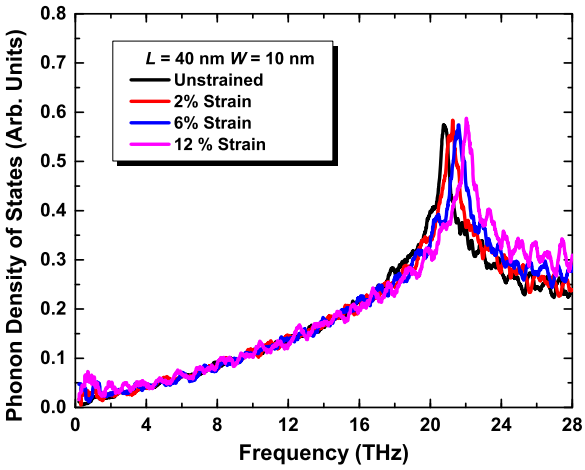

Figure 10. Plot of phonon density of states versus frequency for carbon atoms for a representative system ($L = 40$ nm and $W = 10$ nm) with aspect ratio of 4, focusing on shifting of ZO vibrational mode peak for different degree of applied tensile strain.

figure are a few schematic snapshots of the strained systems in the equilibrated geometry for a clearer visualization. The figure shows two trends which are discussed below.

Under tensile strain, a significant decrease in Λ_2 was observed. Here, several factors play a role which could potentially alter the observed values. First, the areal density of interacting carbon atoms decreases with tensile strain. For example, with a relative strain of 1.1, the areal carbon atom density decreases by a factor of 10% on both GNRs, which in turn results in a ~20% decrease in interaction energy for the same overlap area. Secondly, as discussed above, the increase in aspect ratio (~1.1 times) is also expected to change (~5% increase from figure 3 data) the thermal conductance. While these combined factors could lead to a predicted ~10–20% decrease in thermal conductance values, the observed five-fold decrease can be explained using a bond stiffening argument. It is expected that GNRs become notably stiffer with tensile strain due to stiffening of C-C bonds. This effect of bond stiffening is clearly shown in figure 10 for different applied tensile strain values for the representative studied system ($L = 40$nm and $W = 10$ nm), focusing on out-of-plane optical mode (ZO) [50], occurring ~20 THz. With increasing values of in-plane strain, the figure clearly shows a shift of characteristic vibrational peak towards higher frequencies. This apparent shift to the higher frequency (higher energy) leads to a lower number of interacting phonons (lower amplitude) at studied temperature. Furthermore, the stiffening is expected to increase the group velocity of the phonons and increase their effective mean free path. This, in turn, relatively lessens the number of anharmonic phonon-phonon scattering events, also lowering the effective phonon interaction time across the junction. We argue that both factors (lower number of phonons and lesser interaction time due to bond stiffening) contribute towards observed lowering of thermal conductance with increasing tensile strain.

For *applied* compressive strain, it was observed that the conductance was not noticeably affected. When compressive strain was used to shorten the GNRs along its length direction (by shortening all bond lengths at beginning of the strain), we observed a subsequent relaxation of the GNRs by a resetting of the bonds to their original unstrained lengths. To accommodate such relaxation, the nano-ribbons buckled to some degree (see schematic in figure 9 corresponding to

Distribution A. Approved for public release; distribution unlimited.

a normalized strain ratio of 0.94). Additionally, the contact region was observed to be relatively flat for all buckled cases. Since the areal density of the carbon atoms and the contact area remained very similar even after bucking, we observed that the thermal energy exchange was not noticeably affected, resulting in very similar values of ITC (Λ_2). The observed invariance in Λ_2 is indicative of similar contributions from Λ_i and Λ_o for different degrees of partial GNR buckling. Similar to indifferences in Λ_2 due to studied roughness, the simulations further substantiate that out-of-plane thermal conductance predominantly depends upon phonon characteristics of the interacting region and is indifferent to overall GNR conformations such as partial GNR buckling and their roughness characteristics as discussed before.

Summary and conclusions

The observed thermal transport dependences in GNR crossed-over contacts from MD simulations demonstrate a few important points. GNR aspect ratio is found to be a key physical characteristic which governs the magnitude of thermal energy exchange and thus, thermal conductance. The dependence of aspect ratio, found to be logarithmic in nature, is derived using a phenomenological model, decoupling the contributions from GNR edges and inner atoms within the interacting zone. The invariance of thermal conductance with respect to studied rough GNR indicates that the out-of-plane conductance (Λ_2) is determined by the edge characteristics within the interacting zone and does not noticeably depend on overall GNR roughness features. Furthermore, the temperature and tensile strain dependence on calculated values of thermal conductance is shown to be governed by the number of interacting phonons as well as their retention time across the interacting zone.

We should duly note that because of the classical nature of the performed MD simulations, the effect of electron–phonon interactions was not included in this study. It is likely that for GNRs with metallic or small band gap semiconducting character, the interfacial thermal conductance will be strongly influenced by the electronic conduction as well as electron–phonon interactions in the contact. Furthermore, it is important to note that as the conductance values were calculated in a suspended GNR-pair geometry, their direct incorporation into design rules for supported-GNR based nano-electronics should be performed with cautious, as graphene–substrate interactions (which are neglected here) should also play an important role towards determining the extent of thermal energy exchange and temperature distribution within the system. Nevertheless, we believe that our study provides the first few key steps in that direction from the perspective of *which* intrinsic GNR parameters are of primary importance and the *extent* of modulation in ITC across them.

Acknowledgements

The authors are very grateful to US Air Force Office of Scientific Research (AFOSR) for the financial support (Lab Task # 2306AR8P: PM—Dr Ali Sayir) and Department of Defense Supercomputing Research Center (AFRL-DSRC) for computational time to carry out the simulations.

Distribution A. Approved for public release; distribution unlimited.

References

[1] Sazonova V, Yaish Y, Ustunel H, Roundy D, Arias T A and McEuen P L 2004 *Nature* **431** 284–7
[2] Bunch J S, Van der Zande A M, Verbridge S S, Frank I W, Tanenbaum D M, Parpia J M, Craighead H G and McEuen P L 2007 *Science* **315** 490–3
[3] Cao Q, Kim H-S, Pimparkar N, Kulkarni J P, Wang C, Shim M, Roy K, Alam M A and Rogers J A 2008 *Nature* **454** 495–500
[4] Bell L E 2008 *Science* **321** 1457–61
[5] Reddy P, Jang S-Y, Segalman R and Majumdar A 2007 *Science* **315** 1568–71
[6] Chang C W, Okawa D, Majumdar A and Zettl A 2006 *Science* **314** 1121–4
[7] Saito R, Dresselhaus G and Dresselhaus M S 1998 *Physical Properties of Carbon Nanotubes* (London: Imperial College Press)
[8] Avouris P and Xia F 2012 *MRS Bull.* **37** 1225–33
[9] Pop E, Varshney V and Roy A K 2012 *MRS Bull.* **37** 1279–86
[10] Marconnet A M, Panzer M A and Goodson K E 2013 *Rev. Mod. Phys.* **85** 1295–326
[11] Avouris P 2004 *MRS Bull.* **29** 403–10
[12] Xia F, Farmer D B, Lin Y and Avouris P 2010 *Nano Lett.* **10** 715–8
[13] Kumar S, Alam M A and Murthy J Y 2007 *J. Heat Transfer* **129** 500–8
[14] Lau P H, Takei K, Wang C, Ju Y, Kim J, Yu Z, Takahashi T, Cho G and Javey A 2013 *Nano Lett.* **13** 3864–9
[15] Chandra B, Park H, Maarouf A, Martyna G J and Tulevski G S 2011 *Appl. Phys. Lett.* **99** 072110
[16] Prasher R 2008 *Phys. Rev.* B **77** 075424
[17] Yamada Y, Nishiyama T, Yasuhara T and Takahashi K 2012 *J. Therm. Sci. Tech. -Japan* **7** 190–8
[18] Yang J, Waltermire S, Chen Y, Zinn A A, Xu T T and Li D 2010 *Appl. Phys. Lett.* **96** 023109
[19] Cola B A, Xu J, Cheng C, Xu X, Hu H and Fisher T S 2007 *J. Appl. Phys.* **101** 054313
[20] Koh Y K, Bae M-H, Cahill D G and Pop E 2010 *Nano Lett.* **10** 4363–8
[21] Mao R, Kong B D, Kim K W, Jayasekera T, Calzolari A and Nardelli M B 2012 *Appl. Phys. Lett.* **101** 113111
[22] Prasher R S, Hu X J, Chalopin Y, Mingo N, Lofgreen K, Volz S, Cleri F and Keblinski P 2009 *Phys. Rev. Lett.* **102** 105901
[23] Evans W J, Shen M and Keblinski P 2012 *Appl. Phys. Lett.* **100** 261908
[24] Evans W J and Keblinski P 2010 *Nanotechnology* **21** 475704
[25] Zhong H and Lukes J R 2006 *Phys. Rev.* B **74** 125403
[26] Maruyama S, Igarashi Y, Taniguchi Y and Shiomi J 2006 *J. Therm. Sci. Tech. -Japan* **1** 138–48
[27] Xu Z and Buehler M J 2009 *ACS Nano* **3** 2767–75
[28] Konatham D, Papavassiliou D and Striolo A 2012 *Chem. Phys. Lett.* **527** 47–50
[29] Wei Z, Ni Z, Bi K, Chen M and Chen. Y 2012 *Phys. Lett.* A **375** 1195–9
[30] Sun K, Stroscio M A and Dutta M 2009 *Superlattices Microstruct.* **45** 60–4
[31] Ni Y, Chalopin Y and Volz S 2012 *J. Phys.: Conf. Ser.* **395** 012106
[32] Varshney V, Patnaik S S, Roy A K and Farmer B L 2010 *J. Phys. Chem.* C **114** 16223–8
[33] Bui K, Grady B P and Papavassiliou D V 2011 *Chem. Phys. Lett.* **508** 248–51
[34] Gengler J J, Shenogin S V, Bultman J E, Roy A K, Voevodin A A and Muratore C 2012 *J. Appl. Phys.* **112** 094904
[35] Roy A K, Farmer B L, Varshney V, Sihn S, Lee J and Ganguli S 2012 *ACS Appl. Mater. Interfaces* **4** 545–63
[36] Bagri A, Kim S-P, Ruoff R S and Shenoy V B 2011 *Nano Lett.* **11** 3917–21
[37] Chen Z, Jang W, Bao W, Lau C N and Dames C 2009 *Appl. Phys. Lett.* **95** 161910
[38] Wang H, Gong J, Pei Y and Xu Z 2013 *ACS Appl. Mater. Interfaces* **5** 2599–603
[39] Hu M and Poulikakos D 2013 *Int. J. Heat Mass Tranfer* **62** 205–13
[40] Plimpton S 1995 *J. Comput. Phys.* **117** 1–19
[41] Sun H, Mumby S J, Maple J R and Hagler A T 1994 *J. Am. Chem. Soc.* **116** 2978–87
[42] Huxtable S T *et al* 2003 *Nat. Mater.* **2** 731–4

Distribution A. Approved for public release; distribution unlimited.

[43] Shenogin S, Xue L, Ozisik R, Keblinski P and Cahill D G 2004 *J. Appl. Phys.* **95** 8136–44
[44] Hu M, Keblinski P, Wang J S and Raravikar N 2008 *J. Appl. Phys.* **104** 083503
[45] Clancy T C and Gates T S 2006 *Polymer* **47** 5990–6
[46] Liu J, Alhashme M and Yang R 2012 *Carbon* **50** 1063–70
[47] Varshney V, Lee J, Roy A K and Farmer B L 2011 *J. Appl. Phys.* **109** 084913
[48] Lee J, Varshney V, Roy A K and Farmer B L 2011 *J. Chem. Phys.* **135** 104109
[49] Varshney V, Roy A K, Dudis D S, Lee J and Farmer B L 2012 *Nanoscale* **4** 5009–16
[50] Sanders G D, Nugraha A R T, K Sato K, Kim J-H, Kono J, Saito R and Stanton C J 2013 *J. Phys.: Condens. Matter* **25** 144201

Distribution A. Approved for public release; distribution unlimited.